J Intell Robot Syst (2012) 67:61–73
DOI 10.1007/s10846-012-9650-4

A Diagnostic Thau Observer for a Class of Unmanned Vehicles

Alessandro Freddi · Sauro Longhi · Andrea Monteriù

Received: 17 June 2011 / Accepted: 2 January 2012 / Published online: 14 January 2012

Abstract This paper addresses the problem of sensor fault detection for a wide class of Unmanned Vehicles (UVs). First a general model for UVs, based on the dynamics of a 6 Degrees Of Freedom (6-DOF) rigid body, subject to gravity and actuation forces, is presented. This model is shown to satisfy the necessary conditions to the existence of a non-linear observer (Thau) when proper assumptions for the actuation forces are made. The observer can thus be used to generate diagnostic residuals inside a Fault Detection (FD) system. Finally, the proposed approach is customized for sensor fault detection on an unmanned quad-rotor vehicle, and simulation results show the effectiveness of the adopted solution.

Keywords Model-based fault diagnosis · Fault detection · Quad-rotor dynamics · Observers

A. Freddi · S. Longhi (✉) · A. Monteriù
Dipartimento di Ingegneria dell'Informazione, Università Politecnica delle Marche, Via Brecce Bianche, Monte Dago, 60131 Ancona, Italy
e-mail: sauro.longhi@univpm.it

A. Freddi
e-mail: freddi@diiga.univpm.it

A. Monteriù
e-mail: a.monteriu@univpm.it

1 Introduction

In the last decades, autonomous unmanned aerial, underwater and ground vehicles have generated considerable attraction due to their strong autonomy and ability to perform relatively difficult tasks in remote, uncertain or hazardous environments where humans are unable to go.

The purposes of such Unmanned Vehicles (UVs) are extremely various, ranging from scientific exploration and data collection, to provision of commercial services, military reconnaissance and intelligence gathering. A number of UV systems have become available and research is ongoing in a number of areas that will significantly advance the state of the art in UV technology. Moreover designers have more freedom in the development of such vehicles, not having to account for the presence of a pilot and the associated life-support systems. This potentially results in cost and size savings, as well as increased operational capabilities [9, 12].

Since these vehicles operate in an environment subjected to a high degree of uncertainties and disturbances, the problem of precise and accurate control and estimation of these vehicles is difficult and requires advanced control and estimation theories [3, 8, 25]. On the other hand, with an increasing requirement for control systems to be more secure and reliable, fault diagnosis and tolerance

in such control systems is becoming more and more critical and significant [21].

Strong autonomy implies the ability of each unmanned vehicle to work properly and safely for a long time, and thus to successfully complete the mission. In presence of undesirable effects such as faults in the actuators or sensors, the vehicles control systems must be responsive and adaptive to such faults [10]. Specifically, one is required to develop an autonomous fault diagnosis, health monitoring and reconfigurable control systems.

An ad-hoc Fault Detection (FD) system is usually developed for the specific UV under consideration, with the result that the developed diagnostic system cannot be used for other UVs. This paper deals with developing an observer-based diagnostic system for a wide class of UVs, exploiting the knowledge of the non-linear mathematical model, used as a faithful replica of the UV dynamics. The main problem to deal with is that the nonlinearity of the UV model does not permit to exploit the significant developments which have been made in the area of model-based fault detection in linear systems [4]. The proposed model-based approach makes use of a Thau observer [4, 17, 24] to generate diagnostic signals - residuals. In the framework of fault diagnosis, faults are detected by setting a variable threshold on each residual signal. The subsequent analysis of each residual, once a threshold is exceeded, then leads to fault detection [16]. This represents the essential information for developing an effective fault tolerant system for a wide class of UVs.

The contribution of this paper is to successfully develop and apply a well-known diagnostic observer technique to a wide class of UVs (aerial, underwater or ground) modelled with a general non-linear model in which each vehicle is considered as a six Degrees Of Freedom (6-DOF) rigid body subject to gravity and actuation forces. This model can be adapted to a specific application simply specifying the physical parameters and the actuation forces which do not alter the Lipschitz properties of the model. In this way a full order Thau observer [4] can be built to generate residuals to be used inside a FD system. In faultless situations, residuals remain around zero, while if a fault occurs, their values change, permitting to detect the fault.

A four-rotor aerial vehicle, known as quadrotor, is considered here to show the effectiveness of the proposed diagnostic system which is capable of detecting faults on the onboard inertial measurement unit. A quad-rotor is an underactuated system with four independent inputs and six coordinate outputs. This vehicle has been chosen by many researchers as a very promising vehicle for indoor/outdoor navigation [1, 2, 13, 23].

The paper is organized as follows. In Section 2, the nonlinear model for a wide class of unmanned vehicles is derived and presented. The fault detection system is described and developed for the considered class of UVs in Section 3. Section 4 is devoted to the presentation of the simulation results obtained for various fault scenarios when the proposed fault detection scheme is applied to a particular UV system, namely a four-rotor aerial vehicle. Conclusions and future directions are presented at the end of the paper.

2 Mathematical Model for Unmanned Vehicles

In this section a general model for a wide class of UVs, suitable for the construction of a Thau observer for FD purposes, is proposed. The UV is regarded as a 6-DOF rigid body subject to gravity and actuation forces. The solution which will be described in the next section, is thus suitable for UVs whose dynamics can be manly described using the rigid body approximation subject to gravity and actuation forces, as long as the assumptions described below are satisfied. The rigid body dynamics is described using an Euler-Lagrangian formulation in which three assumptions are made. These assumptions allow to derive a simple model which, at the same time, is complex enough to account for the major dynamics of a rigid body moving freely in all the six degrees of freedom.

Two frames are used to study the system motion: an inertial earth frame $\{R_E\}$ (O, x, y, z), and a body-fixed frame $\{R_B\}$ $\{O_B, x_B, y_B, z_B\}$.

Assumption 1 O_B is placed at the center of mass of the rigid body.

In this way $\{R_B\}$ is related to $\{R_E\}$ by a position vector $\boldsymbol{\xi} = \begin{bmatrix} x & y & z \end{bmatrix}^T$, describing the position of the center of gravity in $\{R_B\}$ with respect to $\{R_E\}$ and by a vector of three independent angles $\boldsymbol{\eta} = \begin{bmatrix} \phi & \theta & \psi \end{bmatrix}^T$, respectively roll, pitch and yaw, which represent the orientation of the body-fixed frame $\{R_B\}\{O_B, x_B, y_B, z_B\}$ with respect to the earth frame $\{R_E\}(O, x, y, z)$. The adopted notation is based on the assumption that the earth frame $\{R_E\}(O, x, y, z)$ can reach the same orientation of the body-fixed frame $\{R_B\}\{O_B, x_B, y_B, z_B\}$ by first performing a rotation of an angle ψ around the z-axis (yaw), then a rotation of an angle θ around the new y-axis (pitch) and finally a rotation of an angle ϕ around the new x-axis (roll). All the rotations are right-handed with $\left(-\frac{\pi}{2} \ll \phi \ll \frac{\pi}{2}\right)$, $\left(-\frac{\pi}{2} \ll \theta \ll \frac{\pi}{2}\right)$, and ψ is unrestricted. Note that the considered UVs usually work with much more conservative angles and the above constraints on ϕ and θ are widely satisfied in common real applications, and thus should be seen as an unreacheable limit.

The translational kinetic energy of the vehicle is expressed as [22]

$$T_{\text{trans}} \triangleq \frac{1}{2} m \dot{\boldsymbol{\xi}}^T \dot{\boldsymbol{\xi}} \tag{1}$$

where m denotes the whole mass of the rigid body.

The rotational kinetic energy is given by [19]

$$T_{\text{rot}} \triangleq \frac{1}{2} \dot{\boldsymbol{\eta}}^T \mathbf{J} \dot{\boldsymbol{\eta}} \tag{2}$$

where $\mathbf{J}$ is the inertia matrix expressed directly in terms of the generalized coordinates $\boldsymbol{\eta}$

$$\mathbf{J} = \mathbf{W}_{\eta}^T \mathbf{I} \mathbf{W}_{\eta} \tag{3}$$

with

$$\mathbf{W}_{\eta} = \begin{bmatrix} 1 & 0 & -S_{\theta} \\ 0 & C_{\phi} & S_{\phi} C_{\theta} \\ 0 & -S_{\phi} & C_{\phi} C_{\theta} \end{bmatrix} \tag{4}$$

where $S_{(.)}$ and $C_{(.)}$ represent $\sin(.)$ and $\cos(.)$ respectively, and $\mathbf{I}$ is the moment of inertia tensor.

Assumption 2 The body frame axis are the principal inertia axis of the rigid body.

With this assumption one can express matrix $\mathbf{I}$ as a diagonal matrix

$$\mathbf{I} \triangleq \begin{bmatrix} I_{xx} & 0 & 0 \\ 0 & I_{yy} & 0 \\ 0 & 0 & I_{zz} \end{bmatrix}, \tag{5}$$

and thus

$$\mathbf{J} = \begin{bmatrix} I_{xx} & 0 & -I_{xx} S_{\theta} \\ 0 & I_{yy} C_{\phi}^2 + I_{zz} S_{\phi}^2 & \left(I_{yy} - I_{zz}\right) S_{\phi} C_{\phi} C_{\theta} \\ -I_{xx} S_{\theta} & \left(I_{yy} - I_{zz}\right) & I_{xx} S_{\theta}^2 + I_{yy} S_{\phi}^2 C_{\theta}^2 \\ & \times & S_{\phi} C_{\phi} C_{\theta} \qquad + I_{zz} C_{\phi}^2 C_{\theta}^2 \end{bmatrix}. \tag{6}$$

The only potential energy which needs to be considered is due to the gravitational field. Therefore, potential energy is expressed as

$$U = mgz\,. \tag{7}$$

Let $\mathbf{q} = \begin{bmatrix} \boldsymbol{\xi}^T & \boldsymbol{\eta}^T \end{bmatrix}^T = [x, y, z, \phi, \theta, \psi]^T \in \mathbb{R}^6$ be the generalized coordinates vector for the rigid body, the Lagrangian is given by

$$\begin{aligned} \mathcal{L}(\mathbf{q}, \dot{\mathbf{q}}) &= T_{\text{trans}} + T_{\text{rot}} - U = \\ &= \frac{1}{2} m \dot{\boldsymbol{\xi}}^T \dot{\boldsymbol{\xi}} + \frac{1}{2} \dot{\boldsymbol{\eta}}^T \mathbf{J} \dot{\boldsymbol{\eta}} - mgz \\ &= \frac{1}{2} m \dot{\mathbf{q}}^T \mathbf{M} \dot{\mathbf{q}} + \frac{1}{2} \dot{\mathbf{q}}^T \mathbf{N} \dot{\mathbf{q}} - \mathbf{o}^T \mathbf{q} \end{aligned}$$

where $\boldsymbol{M} = \begin{bmatrix} \boldsymbol{I}_{3\times3} & \mathbf{0}_{3\times3} \\ \mathbf{0}_{3\times3} & \mathbf{0}_{3\times3} \end{bmatrix}$, $\boldsymbol{N} = \begin{bmatrix} \mathbf{0}_{3\times3} & \mathbf{0}_{3\times3} \\ \mathbf{0}_{3\times3} & \mathbf{J} \end{bmatrix}$ and $\mathbf{o} = \begin{bmatrix} 1 & 1 & mg & 1 & 1 & 1 \end{bmatrix}^T$.

The model for the vehicle dynamics is obtained from the Euler-Lagrange equations with external generalized force $\mathbf{F}_E \doteq \begin{bmatrix} \mathbf{F}_{\boldsymbol{\xi}}^T & \boldsymbol{\tau}_{\eta}^T \end{bmatrix}^T$:

$$\frac{d}{dt}\left(\frac{\partial \mathcal{L}}{\partial \dot{\mathbf{q}}}\right) - \frac{\partial \mathcal{L}}{\partial \mathbf{q}} = \mathbf{F}_E \tag{8}$$

$\mathbf{F}_{\xi}$ defines the translational force applied to the rigid body due to the control inputs and relative to the frame $\{R_E\}$, and $\boldsymbol{\tau}_{\eta}$ is the generalized torques vector.

Denoting with $\mathbf{F}_0$ the translational force applied to the rigid body due to the control inputs

and with $\boldsymbol{\tau}_\omega$ the torques vector, both expressed using the body frame coordinates, one can write:

$$\mathbf{F}_\xi = \mathbf{R}_{BE}\mathbf{F}_0 \tag{9a}$$

$$\boldsymbol{\tau}_\eta = \mathbf{R}_{BE}\boldsymbol{\tau}_\omega \tag{9b}$$

where $\mathbf{R}_{BE}$ is the rotation matrix which allow to express in earth frame coordinates a vector previously expressed using the body frame coordinates.

$$\mathbf{R}_{BE} = \begin{bmatrix} C_\theta C_\psi & C_\psi S_\theta S_\phi - C_\phi S_\psi & C_\phi C_\psi S_\theta + S_\phi S_\psi \\ C_\theta S_\psi & S_\theta S_\phi S_\psi + C_\phi C_\psi & C_\phi S_\theta S_\psi - C_\psi S_\phi \\ -S_\theta & C_\theta S_\phi & C_\theta C_\phi \end{bmatrix}. \tag{10}$$

Note that for a generic rigid body evolving in space, both $\mathbf{F}_0$ and $\boldsymbol{\tau}_\omega$ should depend on $\boldsymbol{\xi}$, $\boldsymbol{\eta}$ and the system input vector, namely $\boldsymbol{u}$.

Assumption 3 The contribution of the small body forces (Euler, centrifugal and Coriolis) to the set of equation describing the translational dynamics is neglectable.

This assumption implies that the Lagrangian contains no cross-terms in the kinetic energy combining $\dot{\boldsymbol{\xi}}$ and $\dot{\boldsymbol{\eta}}$ [3], thus the Euler-Lagrange equation can be partitioned into the dynamics for the $\boldsymbol{\xi}$ coordinates and the dynamics for the $\boldsymbol{\eta}$ coordinates:

$$m\ddot{\boldsymbol{\xi}} + \begin{bmatrix} 0 \\ 0 \\ mg \end{bmatrix} = \mathbf{F}_\xi \tag{11a}$$

$$\mathbf{J}\ddot{\boldsymbol{\eta}} + \dot{\mathbf{J}}\dot{\boldsymbol{\eta}} - \frac{1}{2}\frac{\partial}{\partial \boldsymbol{\eta}}\left(\dot{\boldsymbol{\eta}}^T\mathbf{J}\right)\dot{\boldsymbol{\eta}} = \boldsymbol{\tau}_\eta \tag{11b}$$

Defining the Coriolis matrix as

$$\mathbf{F}_c(\boldsymbol{\eta}, \dot{\boldsymbol{\eta}}) = \dot{\mathbf{J}} - \frac{1}{2}\frac{\partial}{\partial \boldsymbol{\eta}}\left(\dot{\boldsymbol{\eta}}^T\mathbf{J}\right) \tag{12}$$

the expression 11b can be rewritten as

$$\mathbf{J}\ddot{\boldsymbol{\eta}} + \mathbf{F}_c(\boldsymbol{\eta}, \dot{\boldsymbol{\eta}})\dot{\boldsymbol{\eta}} = \boldsymbol{\tau}_\eta \tag{13}$$

where

$$\mathbf{F}_c(\boldsymbol{\eta}, \dot{\boldsymbol{\eta}}) = \begin{bmatrix} F_{11} & F_{12} & F_{13} \\ F_{21} & F_{22} & F_{23} \\ F_{31} & F_{32} & F_{33} \end{bmatrix} \tag{14}$$

and

$$F_{11} = 0 \tag{15a}$$

$$F_{12} = \frac{1}{2}\left(-\dot{\psi}c_\theta c_\phi^2 + 2\dot{\theta}c_\phi s_\phi + \dot{\psi}c_\theta s_\phi^2\right)\left(I_{yy} - I_{zz}\right) \tag{15b}$$

$$F_{13} = -\dot{\theta}c_\theta I_{xx} - \frac{1}{2}c_\theta\left(\dot{\theta}c_\phi^2 + 2\dot{\psi}c_\theta c_\phi s_\phi - \dot{\theta}s_\phi^2\right)\left(I_{yy} - I_{zz}\right) \tag{15c}$$

$$F_{21} = \frac{1}{2}\dot{\psi}c_\theta I_{xx} \tag{15d}$$

$$F_{22} = -2\dot{\phi}c_\phi s_\phi\left(I_{yy} - I_{zz}\right) + \frac{1}{2}\dot{\psi}c_\phi s_\theta s_\phi\left(I_{yy} - I_{zz}\right) \tag{15e}$$

$$F_{23} = \left(\dot{\phi}c_\theta c_\phi^2 - \dot{\theta}c_\phi s_\theta s_\phi - \dot{\phi}c_\theta s_\phi^2\right)\left(I_{yy} - I_{zz}\right) + \frac{1}{2}\left(\dot{\phi}c_\theta I_{xx} - 2\dot{\psi}c_\theta s_\theta I_{xx} + \dot{\theta}c_\phi s_\theta s_\phi I_{yy} + 2\dot{\psi}c_\theta s_\theta s_\phi^2 I_{yy} + 2\dot{\psi}c_\theta c_\phi^2 s_\theta I_{zz} - \dot{\theta}c_\phi s_\theta s_\phi I_{zz}\right) \tag{15f}$$

$$F_{31} = -\dot{\theta}c_\theta I_{xx} \tag{15g}$$

$$F_{32} = \left(\dot{\phi}c_\theta c_\phi^2 - \dot{\theta}c_\phi s_\theta s_\phi - \dot{\phi}c_\theta s_\phi^2\right)\left(I_{yy} - I_{zz}\right) \tag{15h}$$

$$F_{33} = 2c_\theta\left(\dot{\theta}s_\theta I_{xx} + \dot{\phi}c_\theta c_\phi s_\phi I_{yy} - \dot{\theta}s_\theta s_\phi^2 I_{yy} - \dot{\theta}c_\phi^2 s_\theta I_{zz} - \dot{\phi}c_\theta c_\phi s_\phi I_{zz}\right). \tag{15i}$$

Since $\mathbf{J}$ is nonsingular, the equations of motion for the rigid body can be finally expressed as

$$m\ddot{\boldsymbol{\xi}} = \mathbf{F}_\xi + \begin{bmatrix} 0 \\ 0 \\ -mg \end{bmatrix} \tag{16a}$$

$$\ddot{\boldsymbol{\eta}} = \mathbf{J}^{-1}\left[\boldsymbol{\tau}_\eta - \mathbf{F}_c(\boldsymbol{\eta}, \dot{\boldsymbol{\eta}})\dot{\boldsymbol{\eta}}\right] \tag{16b}$$

It is our claim that the assumptions made in order to derive the model described by Eqs. 16a and 16b do not imply a significative reduction to the model capability of describing the dynamics of a generic 6-DOF rigid body. In particular, in the Assumption 1, the origin of the body frame can be chosen to coincide with the center of gravity of the body frame whenever the geometry and the mass distribution of the vehicle is well known. This is the case for many UVs with fixed mass.

In Assumption 2, by the spectral theorem, there is always a Cartesian coordinate system in which the inertia tensor is diagonal. It is sufficient to find the suitable coordinate system and use it as the body frame coordinate system. In Assumption 3, neglection of the small body forces allows to obtain a simplified model. This simplification is justified by the fact that in common UVs the effect of actuation forces on the system dynamics is several times greater than that of small body forces.

3 The Fault Detection System

A fault detection system is usually made of two main components: a residual generation module and a residual evaluation module. The residual generation module has the task to use information both from the model and from the actual inputs and outputs of the system to provide a signal whose value should be almost zero when no fault is affecting the system, while it should differ from zero when a fault is present. The residual evaluation module, instead, has the task to provide the correct interpretation of the residual signal in order to reduce (theoretically to zero) the number of false alarms. In this paper we focus our analysis on both residual generation and residual evalution.

The easiest solution when dealing with model-based techniques for residual generation in non-linear systems is to apply linear techniques based on the linearized model of the system around a proper working point. In [6], for instance, the authors realize a number of Auto Regressive eXogenous models to be used for FDI purposes. However this solution is suitable only for those vehicles operating most of the time near the considered conditions. In all the other cases there are two possible solutions: linearizing the system around different operating conditions or using a non-linear model-based approach. Among the non-linear approaches known in literature, one can find the extended and unscented Kalman filters (see, e.g., [18] and [20]), the structural analysis [14] and several non-linear observers for Lipschitz systems [26].

This section describes how to put Eqs. 16a and 16b in a suitable form to apply a Lipschitz nonlinear observer for residual generation, namely the Thau observer, and derives the class of unmanned vehicles to which the proposed solution can be adopted. The obtained residuals can be evaluated using an adaptive threshold policy, built using a linear combination of mean value, variance and a constant value updated on a moving window. The proposed evaluation technique is detailed in Section 3.3.

3.1 Mathematical Model in State Space Form

Let us consider Eqs. 16a and 16b and put them in state space form by choosing $\boldsymbol{x} = [x_1\ x_2\ \ldots\ x_{12}]^T$ as

$$\left[x_1\ x_2\ x_3\ x_4\ x_5\ x_6\right]^T = \left[x\ y\ z\ \phi\ \theta\ \psi\right]^T \tag{17a}$$

$$\left[x_7\ x_8\ x_9\ x_{10}\ x_{11}\ x_{12}\right]^T = \left[\dot{x}\ \dot{y}\ \dot{z}\ \dot{\phi}\ \dot{\theta}\ \dot{\psi}\right]^T \tag{17b}$$

The system dynamics can thus be written as

$$\begin{bmatrix}\dot{x_1}\\ \dot{x_2}\\ \dot{x_3}\end{bmatrix} = \boldsymbol{I}_{3\times3}\begin{bmatrix}x_7\\ x_8\\ x_9\end{bmatrix} \tag{18a}$$

$$\begin{bmatrix}\dot{x_4}\\ \dot{x_5}\\ \dot{x_6}\end{bmatrix} = \boldsymbol{I}_{3\times3}\begin{bmatrix}x_{10}\\ x_{11}\\ x_{12}\end{bmatrix} \tag{18b}$$

$$\begin{bmatrix}\dot{x_7}\\ \dot{x_8}\\ \dot{x_9}\end{bmatrix} = \frac{1}{m}\mathbf{F}_\xi - \begin{bmatrix}0\\ 0\\ g\end{bmatrix} \tag{18c}$$

$$\begin{bmatrix}\dot{x_{10}}\\ \dot{x_{11}}\\ \dot{x_{12}}\end{bmatrix} = \mathbf{J}^{-1}\left(\boldsymbol{\tau}_\eta - \mathbf{F}_c\begin{bmatrix}x_{10}\\ x_{11}\\ x_{12}\end{bmatrix}\right) \tag{18d}$$

where $\boldsymbol{I}_{i\times i}$ is an identity matrix of dimension i. The dynamics can be written in a compact form as:

$$\begin{cases}\dot{\boldsymbol{x}}(t) = \boldsymbol{A}\boldsymbol{x}(t) + \boldsymbol{h}(\boldsymbol{x}(t), \boldsymbol{u}(t))\\ \boldsymbol{y}(t) = \boldsymbol{C}\boldsymbol{x}(t)\end{cases} \tag{19}$$

where $\boldsymbol{A} = \begin{bmatrix}\mathbf{0}_{6\times6} & \boldsymbol{I}_{6\times6}\\ \mathbf{0}_{6\times6} & \mathbf{0}_{6\times6}\end{bmatrix}$, $\boldsymbol{C} = \left[\boldsymbol{I}_{6\times6}\ \mathbf{0}_{6\times6}\right]$ and $\boldsymbol{h}(\boldsymbol{x}, \boldsymbol{u})$ is a vector whose first six components are "0" and the other six components are the right-terms of Eqs. 18c and 18d. The form of the output matrix $\boldsymbol{C}$ implies that linear and angular positions, relative to the earth frame, are accessible.

3.2 Residual Generation

Thau [24] developed an observer for a special class of non-linear systems. This observer has already been applied to the fault detection and isolation of non-linear dynamic systems and uses the following non-linear system model [4]:

$$\begin{cases} \dot{\boldsymbol{x}}(t) = \boldsymbol{A}\boldsymbol{x}(t) + \boldsymbol{B}\boldsymbol{u}(t) + \boldsymbol{h}(\boldsymbol{x}(t), \boldsymbol{u}(t)) + \boldsymbol{F}_1\boldsymbol{\gamma}(t) \\ \boldsymbol{y}(t) = \boldsymbol{C}\boldsymbol{x}(t) + \boldsymbol{F}_2\boldsymbol{\gamma}(t) \end{cases} \tag{20}$$

where $\boldsymbol{x} \in \mathbb{R}^n$ is the state vector, $\boldsymbol{u} \in \mathbb{R}^r$ is the input vector, $\boldsymbol{y} \in \mathbb{R}^p$ is the output vector, $\boldsymbol{\gamma} \in \mathbb{R}^h$ is the fault vector, $\boldsymbol{A}$, $\boldsymbol{B}$ and $\boldsymbol{C}$ are known system matrices with appropriate dimensions, $\boldsymbol{h}(\boldsymbol{x}(t), \boldsymbol{u}(t))$ represents the nonlinearity, and $\boldsymbol{F}_1$ and $\boldsymbol{F}_2$ are known fault entry matrices which represent the effect of faults on the system.

For developing the Thau observer, the system model 20 has to satisfy the two following conditions:

(c1) the pair $(\boldsymbol{C}, \boldsymbol{A})$ must be observable;
(c2) the non-linear function $\boldsymbol{h}(\boldsymbol{x}(t), \boldsymbol{u}(t))$ must be continuously differentiable and locally Lipschitz with constant ϱ, i.e.

$$||\boldsymbol{h}(\boldsymbol{x}_1(t), \boldsymbol{u}(t)) - \boldsymbol{h}(\boldsymbol{x}_2(t), \boldsymbol{u}(t))|| \leq \varrho||(\boldsymbol{x_1} - \boldsymbol{x_2})||, \forall \boldsymbol{x}_1, \boldsymbol{x}_2 \in \mathbb{R}^n . \tag{21}$$

When these two conditions are satisfied, a stable observer for the system 20 has the form

$$\begin{cases} \dot{\hat{\boldsymbol{x}}}(t) = \boldsymbol{A}\hat{\boldsymbol{x}}(t) + \boldsymbol{B}\boldsymbol{u}(t) + \boldsymbol{h}(\hat{\boldsymbol{x}}(t), \boldsymbol{u}(t)) \\ \qquad\qquad + \boldsymbol{K}(\boldsymbol{y}(t) - \hat{\boldsymbol{y}}(\boldsymbol{t})) \\ \hat{\boldsymbol{y}}(t) = \boldsymbol{C}\hat{\boldsymbol{x}}(t) \end{cases} \tag{22}$$

where $\boldsymbol{K}$ is the observer gain matrix defined by

$$\boldsymbol{K} = \boldsymbol{P}_\delta^{-1}\boldsymbol{C}^T . \tag{23}$$

The matrix $\boldsymbol{P}_\delta$ is the solution to the Lyapunov equation

$$\boldsymbol{A}^T\boldsymbol{P}_\delta + \boldsymbol{P}_\delta\boldsymbol{A} - \boldsymbol{C}^T\boldsymbol{C} + \delta\boldsymbol{P}_\delta = \boldsymbol{0} \tag{24}$$

where δ is a positive parameter which is chosen such that Eq. 24 has a positive definite solution.

In order to apply the observer of Eq. 22 to the system described by Eq. 19, it is necessary to state when conditions (c1) and (c2) are satisfied. The following propositions hold true.

Proposition 1 *For the system described by Eq. 19 the pair* $(\boldsymbol{C}, \boldsymbol{A})$ *is observable.*

Proof The observability matrix results

$$\mathcal{O} = \left[\boldsymbol{C}^T \ (\boldsymbol{C}\boldsymbol{A})^T \ (\boldsymbol{C}\boldsymbol{A}^2)^T \cdots (\boldsymbol{C}\boldsymbol{A}^{11})^T\right]^T \tag{25}$$

where $\left[\boldsymbol{C}^T \ (\boldsymbol{C}\boldsymbol{A})^T\right]^T = \boldsymbol{I}_{12}$, while $\boldsymbol{C}\boldsymbol{A}^i = \boldsymbol{0}_{(6\times 12)}$ $(i = 2, \ldots, 11)$. Thus the observability matrix has full rank, and the pair $(\boldsymbol{C}, \boldsymbol{A})$ is observable. □

Condition (c1) is thus always satisfied as long as the system described by Eq. 19 has accessible linear and angular positions relative to the earth frame.

Proposition 2 *Suppose that* $\mathbf{F}_0(\boldsymbol{x}, \boldsymbol{u})$ *and* $\boldsymbol{\tau}_\omega(\boldsymbol{x}, \boldsymbol{u})$ *(see Eq. 9a) are* $\mathcal{C}^1$ *(i.e. the partial derivatives with respect to the state variables exist and are continuous) and that* $\boldsymbol{u}(t)$ *is continuous in t. Then in Eq. 19 the non-linear function* $\boldsymbol{h}(\boldsymbol{x}, \boldsymbol{u})$ *is continuously differentiable and locally Lipschitz with constant* ϱ.

Proof From [7] we know that, given a function $\boldsymbol{f}(t, \boldsymbol{x})$, continuous together with its partial derivatives $\frac{\partial \boldsymbol{f}}{\partial \boldsymbol{x}}(t, \boldsymbol{x})$ on $[a, b] \times \mathbb{D} \subset \mathbb{R}^n$, then $\boldsymbol{f}(t, \boldsymbol{x})$ is locally Lipschitz in $\boldsymbol{x}$ on $[a, b] \times \mathbb{D}$. By definition we know that if a multivariable function is continuously differentiable (i.e. it is of class $\mathcal{C}^1$), then its partial derivatives exist and are continuous. Since the input $\boldsymbol{u}$ is supposed to be continuous in t and the state vector $\boldsymbol{x}$ is continuous in t, then it is sufficient to show that $\boldsymbol{f}(t, \boldsymbol{x})$ is of class $\mathcal{C}^1$ to prove the proposition.

$\boldsymbol{h}(\boldsymbol{x}(t), \boldsymbol{u}(t))$ has thus to be of class $\mathcal{C}^1$. Let us analyze separately Eqs. 18c and 18d. The first term is:

$$\left(\frac{1}{m}\mathbf{F}_\xi - \begin{bmatrix} 0 \\ 0 \\ g \end{bmatrix}\right) = \left(\frac{1}{m}\mathbf{R}_{BE}\mathbf{F}_0(\boldsymbol{x}, \boldsymbol{u}) - \begin{bmatrix} 0 \\ 0 \\ g \end{bmatrix}\right) \tag{26}$$

whose non-constant elements are due to the product of $\mathbf{R}_{BE}$ and $\mathbf{F}_0(\boldsymbol{x}, \boldsymbol{u})$. Since $\mathbf{R}_{BE}$ contains only sine and cosine non-linearities (see Eq. 10), it is of class $\mathcal{C}^\infty$. However, by hypothesis, we assume that $\mathbf{F}_0(\boldsymbol{x}, \boldsymbol{u})$ is of class $\mathcal{C}^1$, and thus the product term expressed in Eq. 18c is of class $\mathcal{C}^1$ too.

Let us analyze the second term (Eq. 18d):

$$\mathbf{J}^{-1}\left(\boldsymbol{\tau}_\eta - \mathbf{F}_c \begin{bmatrix} x_{10} \\ x_{11} \\ x_{12} \end{bmatrix}\right) = \mathbf{J}^{-1}\left(\mathbf{R}_{BE}\boldsymbol{\tau}_\omega - \mathbf{F}_c \begin{bmatrix} x_{10} \\ x_{11} \\ x_{12} \end{bmatrix}\right) \tag{27}$$

As already said before $\mathbf{R}_{BE}$ is of class $\mathcal{C}^\infty$. Matrix $\mathbf{F}_c$ (see Eqs. 15a and 15i) is made of elements which are the algebraic sum of products between

- sine and cosine terms of the state variables x_4, x_5 and x_6;
- the square of sine and cosine terms of the state variables x_4, x_5 and x_6;
- state variables x_8, x_9 and x_{10};

and it is of class $\mathcal{C}^\infty$ too. Matrix $\mathbf{J}^{-1}$ (see Eq. 6) is of class $\mathcal{C}^\infty$ as long as the constraints $(-\phi_l < \phi < \phi_l)$, $(-\theta_l < \theta < \theta_l)$ are satisfied, where $|\phi_l| \ll \frac{\pi}{2}$ and $|\theta_l| \ll \frac{\pi}{2}$. By hypothesis $\boldsymbol{\tau}_\omega$ is of class $\mathcal{C}^1$, thus the term expressed in Eq. 18d is of class $\mathcal{C}^1$. It follows that function $\boldsymbol{h}(\boldsymbol{x}, \boldsymbol{u})$ is continuously differentiable.

□

Condition (c2) is thus satisfied as long as the actuation forces acting on the system are "smooth enough" and time-continuous. This means that UVs with time-continuous inputs and fixed actuators are always good candidates, while UVs whose actuators vary their position in time can result in good candidates depending on the motion of the actuators. It is our belief, however, that most UVs satisfy condition (c2) at least near conservative operating points as usually adopted in many applications (e.g. hover for flying vehicles, straight motion for ground vehicles, etc).

When conditions (c1) and (c2) are satisfied, a Thau observer can be built for FD purposes. Attention must be paid in the choice of the δ value (see Eq. 24), as this value describes how fast the output of the observer converge to the output of the system. A fast converging estimation of the state is not usually desirable for diagnostic purposes, as it may hide the fault effect briefly after its appearance. It is thus necessary to choose the δ value properly. Usually this is achieved using trial and error procedures, according to the application scenario.

3.3 Residual Evaluation

Due to the model uncertainties and measurement noise, in practical situations, the residual is never zero, even when no faults occur [4]. A threshold policy must be then used, to achieve a robust fault detection. Robustness is achieved using adaptive thresholds [15]. These proposed moving thresholds are built using a linear combination of mean value, variance and a constant value updated on a moving window, which must be tuned according to the application using a trial and error approach. The equations used for the generation of the i-th upper threshold Δ_i, and the i-th lower threshold δ_i are:

$$\Delta_i = \frac{K_{1i}}{T}\int_t^{t+T} r_i(\tau)\,d\tau + \frac{K_{2i}}{T}\int_t^{t+T} \times \left(r_i(\tau) - \frac{1}{T}\int_\tau^{\tau+T} r_i(\sigma)\,d\sigma\right)d\tau + K_{3i} \tag{28a}$$

$$\delta_i = \frac{k_{1i}}{T}\int_t^{t+T} r_i(\tau)\,d\tau + \frac{k_{2i}}{T}\int_t^{t+T} \times \left(r_i(\tau) - \frac{1}{T}\int_\tau^{\tau+T} r_i(\sigma)\,d\sigma\right)d\tau + k_{3i} \tag{28b}$$

where k_{1i}, k_{2i} and k_{3i} are the weights for the lower threshold, K_{1i}, K_{2i} and K_{3i} are the weights for the upper threshold and T is the moving window period.

In order to choose properly the values of these parameters, a specific procedure must be followed. First of all, the vehicle (or simulator) must be functioning in a stable position (e.g.: hover for aerial vehicles and no actuation required for ground and marine vehicles) and each residual must be analyzed, such that it is possible to obtain approximate but useful information about the noise and disturbances acting on the vehicle. For

each residual $r_i(t)$, a time serie of length τ_i ($0 < t < \tau_i$) must be collected. Parameters k_{3i} and K_{3i} must be chosen such that the $i-th$ residual is always $k_{3i} < r_i(t) < K_{3i}$ during the specified time serie. From a theoretical point of view, these two parameters include in the threshold the information about noise and disturbance of the vehicle when no dynamics is excited.

The second parameter to choose is T. T is constant and the same for all the residuals. It represents the time window during which the properties of the residual are evaluated to build the threshold. If T is chosen small, then it will quickly follow the residual, however the threshold built upon it would be prone to several false alarms. In a similar way, if T is chosen big, then it will contain a lot of information about the residual and the threshold built upon it would be less prone to false alarms, but the detection time of the FD system would increase due to the slow dynamics of the threshold. The choice of T is thus a trade-off between false alarm rate and detection time.

If the constraint to satisfy implies a restriction on the detection time, then a fault can be simulated (in the sensors of the real system or in the simulator) and T chosen such that the detection time satisfies the time constraint when the parameters k_{3i} and K_{3i} are those chosen before, while k_{1i}, k_{2i} and K_{1i}, K_{2i} are zero. If the constraint to satisfy implies a restriction on the false alarm rate, then a fault can be simulated (in the sensors of the real system or in the simulator) and T chosen such that the false alarm rate satisfies the constraint when the parameters k_{3i} and K_{3i} are those chosen before, while k_{1i}, k_{2i} and K_{1i}, K_{2i} are zero. Note that, once the fault alarm rate has been fixed, than the detection time depends on it, and vice versa, however they can be improved with a proper choice of the remaining parameters k_{1i}, k_{2i} and K_{1i}, K_{2i}. The procedure of simulating a fault on the vehicle and adjust T according to the main constraints on the system is effective (as it will be shown in simulation in the Section 4.2), however it depends on the type of the fault used for the test. The choice of k_{1i}, k_{2i} and K_{1i}, K_{2i}, instead, depends mainly on the type of fault which must be detected. For additive faults, usually k_{1i} and K_{1i} are set close to 1, and k_{2i} and K_{2i} are at least a magnitude order less than k_{1i} and K_{1i}. For multiplicative faults, k_{2i} and K_{2i} must be greater than k_{1i} and K_{1i}.

Because of its effectiveness, low complexity and high customizability, the proposed threshold process can be applied for residual evaluation of a wide class of unmanned vehicles scenarios.

4 The Quad-rotor Vehicle: A Case of Study

We decided to test the proposed diagnosis system on a four-rotor aerial vehicle, also called quad-rotor (Figure 1). This vehicle is an interesting and challenging case of study, and it has been chosen by many researchers as a very promising vehicle for indoor/outdoor navigation using multidisciplinary concepts [1, 2, 13, 23].

Before testing the FD system on a real quad-rotor vehicle, aim of our future research activities, we decided to validate it in a simulation scenario, where the real system has been replaced by a simulator based on a complex mathematical model, described in Appendix A.

In order to develop the proposed diagnostic system, the quad-rotor is modeled with Eqs. 18a–18d, and the diagnostic observer (Eq. 22) is built on them.

Note that the simulator dynamics described by the model of Appendix A is more comprehensive than one described by Eqs. 18a–18d. In this way the simulation represents a good testbed to show the robustness against model uncertainty of the proposed FD system.

4.1 Simulation Scenario

A common scenario for a quad-rotor vehicle consists on environment surveillance and data collection. For these purposes, the quad-rotor has to reach desired targets of the considered environment, and has to remain in hovering flight over them. Comparing the duration of hovering flight with respect to that of forward/lateral flight, typically the second one is smaller than the first one. For this reason, in this study we focus on the *quasi* hovering flight conditions. Note that the considered study case is typical for such vehicles but the proposed diagnostic observer can be successfully applied to different scenarios as well.

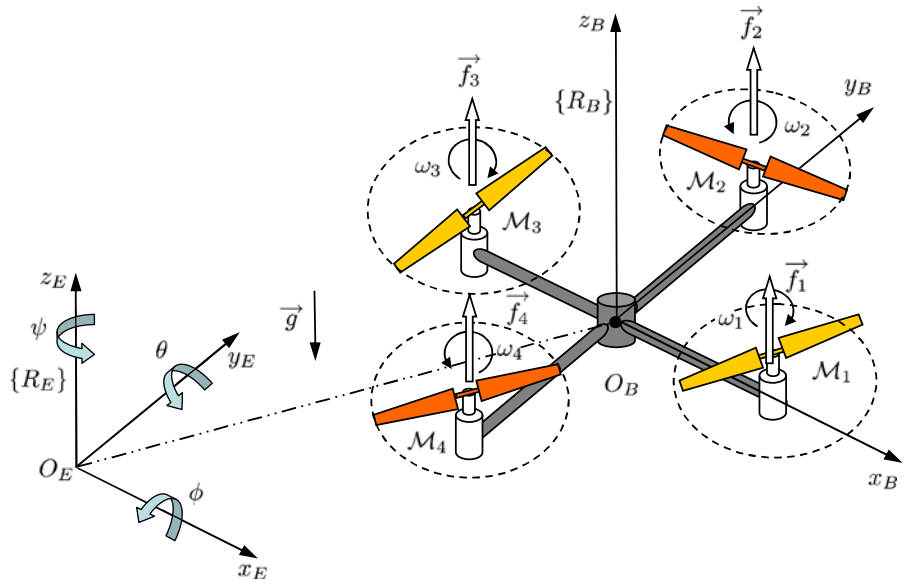

Fig. 1 Quad-rotor rotorcraft

An unmanned quad-rotor system is usually equipped with either a GPS receiver (outdoor operation) or a vision system (indoor flight) and an Attitude and Heading Reference System (AHRS) which provide linear and angular positions of the vehicle. These sensors used in autonomous helicopters can fail in several ways [6]. Some failure types are general for various sensors, while others are specific of a single sensor. In our scenario, the system outputs are the position in the earth frame (x, y and z) and the attitude angles (ϕ, θ and ψ). The faults simulated are additive and incipient (ramp-like faults), and affect the AHRS while the quad-rotor operates in near hover flight conditions as described above.

The residuals are built as the difference between the system outputs and the proposed diagnostic observer outputs, that is to say:

$$r_1(t) = x(t) - \hat{x}(t) \tag{29}$$

$$r_2(t) = y(t) - \hat{y}(t) \tag{30}$$

$$r_3(t) = z(t) - \hat{z}(t) \tag{31}$$

Table 1 Parameters of lower and upper thresholds

	δ_i			Δ_i			
	k_{1i}	k_{2i}	k_{3i}	K_{1i}	K_{2i}	K_{3i}	T_i
$i = 1, 2, 3$	1	0.05	−0.0125	1	0.05	0.0125	12
$i = 4, 5, 6$	1	0.05	−0.05	1	0.05	0.05	12

$$r_4(t) = \phi(t) - \hat{\phi}(t) \tag{32}$$

$$r_5(t) = \theta(t) - \hat{\theta}(t) \tag{33}$$

$$r_6(t) = \psi(t) - \hat{\psi}(t) \tag{34}$$

which are supposed almost zero as long as there are no faults on the sensors and are different from zero in case of faults. In practical situations, due to the measurement noise and disturbances, the residuals are never zero even no faults occur. For brevity we focus the analysis on residuals r_1, r_2, r_3 and r_4 since residuals r_5 and r_6 behave very similar to r_4 for the proposed scenario.

The residual evaluation has been implemented according to the proposed procedure described in Section 3.3, where the lower and upper thresholds have been chosen as shown in Table 1.

4.2 Simulation Results

The non-linear quad-rotor system along with the diagnostic observer have been simulated using the Matlab and Simulink® software. The GPS or vision system model has not been implemented in the simulator since it is considered to be unaffected by fault during the simulations, while the AHRS is supposed to be subject to faults and has been modeled taking into account sampling, quantization error and noise according to the

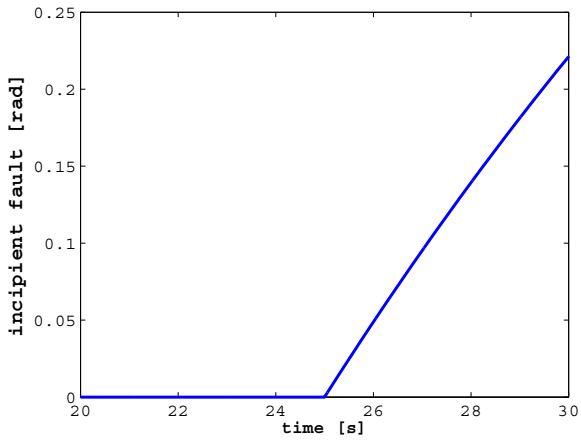

Fig. 2 Fault affecting the AHRS

data-sheet of the Microstrain® 3DM-GX1 [11], which is a widely known, low weight and low cost AHRS. The faults simulated are additive and incipient (ramp-like faults), and affect the system at $t_f = 25s$ while the quad-rotor operates in near hover flight conditions. The analysis of the residuals is performed on r_1, r_2, r_3 and r_4 since residuals r_5 and r_6 behave very similar to r_4 for the proposed scenario.

4.2.1 Fault on the AHRS Roll Output

In the first simulation scenario an incipient ramp-like fault, whose behavior is shown in Fig. 2, affects the roll angle measure of the AHRS, while all other measurements are not affected by any fault. As it can be seen in Fig. 3, residual r_1 is always between the adaptive upper and lower thresholds, and thus showing that longitudinal motion is almost unaffected by the AHRS roll fault. Similarly, residual r_4 remains between the two thresholds, but in this case the residual behavior is due to the noise which is responsible to hide the fault. Residual r_3 is inside the fault free band showing that altitude is not sensitive to the simulated fault. Differently for residual r_2, it can be observed that it crosses the upper threshold, confirming that it is sensitive to the AHRS roll fault. Moreover, this residual behavior shows that the lateral motion is the most affected in case of a fault on the roll sensor.

4.2.2 Fault on the AHRS Pitch Output

In the second simulation scenario an incipient ramp-like fault affects the pitch angle measure

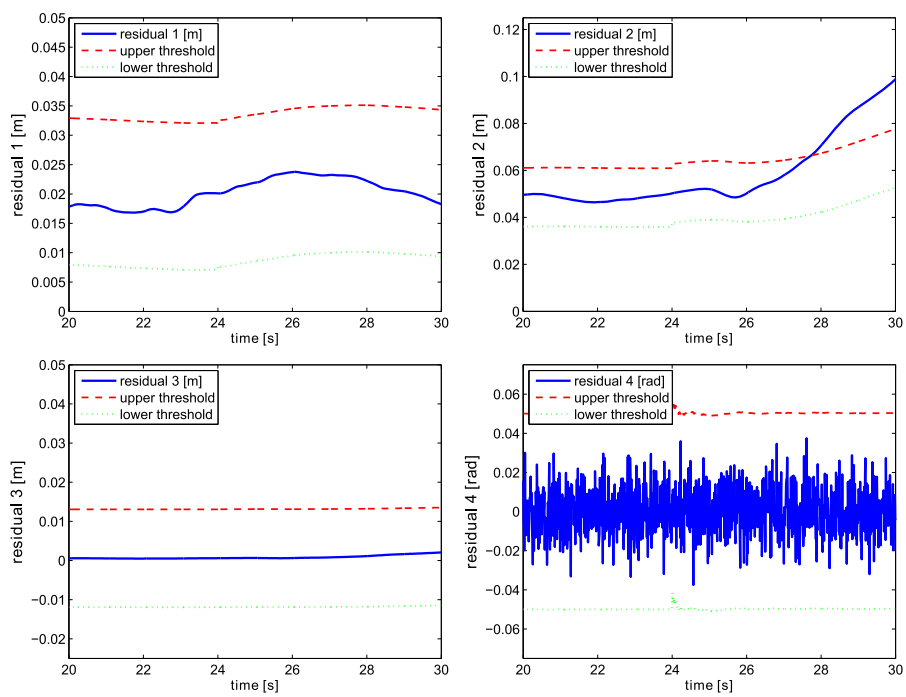

Fig. 3 Residuals in case of fault on AHRS roll channel

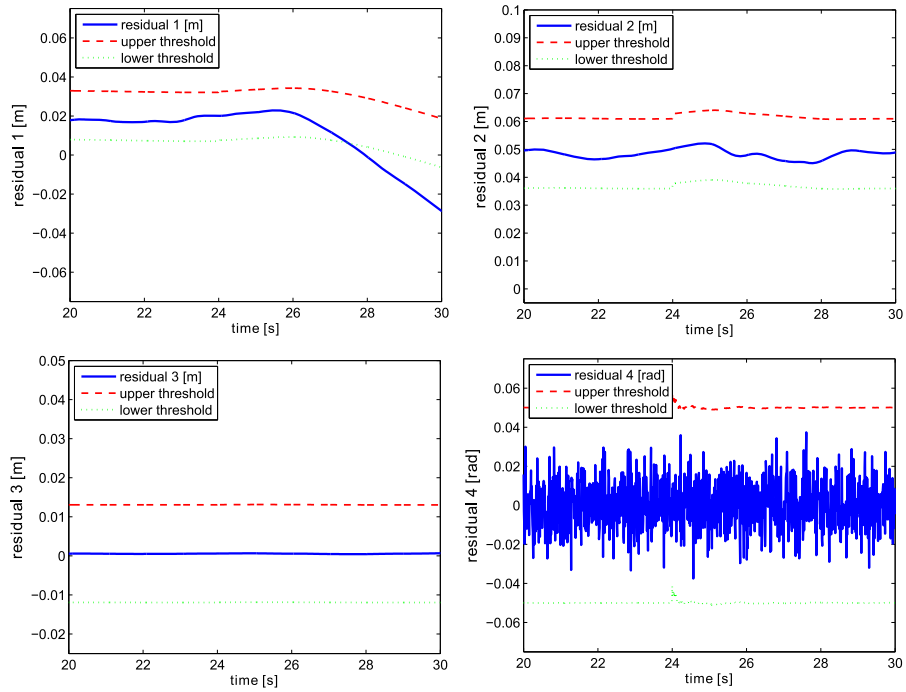

Fig. 4 Residuals in case of fault on AHRS pitch channel

of the AHRS, while all other measurements are not affected by any fault. As it can be seen in Fig. 4, residual r_1 crosses the lower threshold, and it is sensitive to the fault, thus showing that the longitudinal motion is the most affected in case of a fault on the pitch sensor. Residual r_2 is always between the adaptive upper and lower thresholds, and this shows that lateral motion is almost unaffected by the AHRS pitch fault. Considerations about residuals r_3 and r_4 are identical to those stated for the previous simulation scenario.

5 Concluding Remarks

Autonomous vehicles are becoming very popular and play an important role in an increased number of applications, due to their strong autonomy and ability to perform relatively difficult tasks in remote, uncertain or hazardous environments where humans are unable to go. In order to complete their missions in a safer manner, a key requirement for these UVs is the ability to be responsive and adaptive in case of undesirable effects such as faults in the actuators or sensors. An ad-hoc fault detection system is usually developed for the specific UV under consideration, with the result that the developed diagnostic system cannot be used for other UVs.

In this paper, an observer-based diagnostic scheme for the detection of faults has been presented for a wide class of UVs (aerial, underwater or ground). For this class of vehicles, a general model has been proposed, which only needs parameter tuning for the specific application. This is achieved modelling the UV as a 6-DOF rigid body subject to gravity and actuation forces. With this formulation, the model is shown to be useful for diagnosis purposes by exploiting its Lipschitzianity properties. In this way a full order Thau observer has been developed to generate residuals to be used inside the fault detection system. This also represents an essential information for further developing an effective fault tolerant system for a wide class of UVs. A residual evaluation policy has been proposed and validated through simulation trials. The proposed diagnostic scheme has been validated making use of a four-rotor aerial vehicle, known as quad-rotor. The developed FD system is capable of detecting sensor faults on the

onboard inertial measurement unit. The simulation results show the effectiveness of the proposed fault diagnostic scheme.

Providing useful information on the actuation forces, actuator fault detection can be achieved too. Moreover, the proposed FD architecture can be improved introducing a smart threshold generator algorithm, based on a bank of filters, and a fault-tolerant control policy. All of these challenging aspects are currently under investigation. Validation of the proposed diagnostic solution adopting a real vehicle is the aim of the next future research.

Appendix A

Using the well known rigid body equations [5], the quad-rotor simulator, which includes small body forces, translational and rotational drag, is expressed by

$$\begin{cases} \ddot{x} = \frac{1}{m}\left[(C_\phi C_\psi C_\theta + S_\phi S_\psi)u_f - k_t\dot{x}^2\right] \\ \ddot{y} = \frac{1}{m}\left[(C_\phi S_\theta s_\psi - C_\psi s_\phi)u_f - k_t\dot{y}^2\right] \\ \ddot{z} = \frac{1}{m}\left[(C_\theta C_\phi)u_f - mg - k_t\dot{z}^2\right] \\ \dot{p} = \frac{1}{I_{xx}}\left[-k_r p^2 - qr(I_{zz} - I_{yy}) + \tau_p\right] \\ \dot{q} = \frac{1}{I_{yy}}\left[-k_r q^2 - pr(I_{xx} - I_{zz}) + \tau_q\right] \\ \dot{r} = \frac{1}{I_{zz}}\left[-k_r r^2 - pq(I_{yy} - I_{xx}) + \tau_r\right] \\ \dot{\phi} = p + qS_\phi t_\theta + rC_\phi T_\theta \\ \dot{\theta} = qC_\phi - rS_\phi \\ \dot{\psi} = \frac{1}{C_\theta}\left[qS_\phi + rC_\phi\right] \end{cases} \tag{35}$$

where $S_{(.)}$, $C_{(.)}$ and $T(.)$ denote $\sin(.)$, $\cos(.)$ and $\tan(.)$ respectively, $\boldsymbol{\omega} = \left[p, q, r\right]^T$ is the rotational velocity with respect to the body frame axis, k_t is the translational drag, k_r is the rotational drag, $\mathbf{F}_0 = \left[0, 0, u_f\right]^T$ is the force acting on the quad-rotor expressed using the body frame coordinates and $\boldsymbol{\tau}_\omega = \left[\tau_p, \tau_q, \tau_r\right]^T$ is the torque vector expressed using the body frame coordinates (see Fig. 1).

Denoting with f_1, f_2, f_3 and f_4 the forces provided by the rotors along z_B, one can write

$$\begin{cases} u_f = f_1 + f_2 + f_3 + f_4 \\ \tau_p = l\,(f_4 - f_2) \\ \tau_q = l\,(f_3 - f_1) \\ \tau_r = l\,(f_1 - f_2 + f_3 - f_4) \end{cases} \tag{36}$$

References

1. Altug, E., Ostrowski, J.P., Mahony, R.: Control of a quadrotor helicopter using visual feedback. In: Proc. of IEEE Int. Conf. on Robotics and Automation (2002)
2. Bethke, B., Valenti, M., How, J.P.: Uav task assignment. IEEE Trans. Robot. Autom. **15**(1), 39–44 (2008)
3. Castillo, P., Lozano, R., Dzul, A.E.: Modelling and control of mini-flying machines. AIC Advances in Industrial Control. Springer (2005)
4. Chen, J., Patton, R.J.: Robust Model-based Fault Diagnosis for Dynamic Systems. Kluwer Academic Publishers, London (1999)
5. Fossen, T.I.: Marine Control Systems: Guidance, Navigation and Control of Ships, Rigs and Underwater Vehicles. Marine Cybernetics (2002)
6. Heredia, G., Ollero, A., Bejar, M., Mahtani, R.: Sensor and actuator fault detection in small autonomous helicopters. Mechatronics **18**(2):90–99 (2007)
7. Khalil, H.K.: Nonlinear Systems, 3rd edn. Prentice Hall (2002)
8. Leonessa, A.: Underwater robots: motion and force control of vehicle-manipulator systems (g. antonelli; 2006) [book review]. IEEE Control Syst. Mag. **28**(5), 138–139 (2008)
9. Lyon, D.H.: A military perspective on small unmanned aerial vehicles. IEEE Instrum. Meas. Mag. **7**(3), 27–31 (2004)
10. Meskin, N., Khorasani, K.: Actuator fault detection and isolation for a network of unmanned vehicles. IEEE Trans. Automat. Contr. **54**(4), 835–840 (2009)
11. Microstrain. 3DM-GX1 Datasheet (2010)
12. Mohr, B.B., Fitzpatrick, D.L.: Micro air vehicle navigation system. IEEE Aerosp. Electron. Syst. Mag. **23**(4), 19–24 (2008)
13. Mokhtari, A., Benallegue, A.: Dynamic feedback controller of euler angles and wind parameters estimation for a quadrotor unmanned aerial vehicle. In: Proceedings of IEEE International Conference on Robotics and Automation, vol. 3, pp. 2359–2366 (2004)
14. Monteriu, A., Asthan, P., Valavanis, K., Longhi, S.: Model-based sensor fault detection and isolation system for unmanned ground vehicles: theoretical aspects (part i). In: 2007 IEEE International Conference on Robotics and Automation, pp. 2736–2743 (2007)
15. Monteriù, A., Asthana, P., Valavanis, K.P., Longhi, S.: Real-time model-based fault detection and isolation for ugvs. J. Intell. Robot. Syst. **56**(4), 425–439 (2009)

16. Patton, R.J., Frank, P.M., Clark, R.N.: Fault diagnosis in dynamic systems: theory and application. Prentice-Hall, Inc. (1989)
17. Patton, R.J., Frank, P.M., Clark, R.N.: Issues of Fault Diagnosis for Dynamic Systems. Springer (2000)
18. Qi, J., Jiang, Z., Zhao, X., Han, J.: UKF-based rotorcraft UAV Fault adaptive control for actuator failure. In: ROBIO 2007 IEEE International Conference on Robotics and Biomimetics, 2007, pp. 1545–1550 (2007)
19. Raffo, G.V., Ortega, M.G., Rubio, F.R.: An integral predictive/nonlinear H_∞ control structure for a quadrotor helicopter. Automatica **46**(1):29–39 (2010)
20. Rago, C., Prasanth, R., Mehra, R.K., Fortenbaugh, R., S.S.C. Inc, Woburn, M.A.: Failure detection and identification and fault tolerant control using the IMM-KF with applications to the Eagle-Eye UAV. In: Proceedings of the 37th IEEE Conference on Decision and Control, 1998, vol. 4 (1998)
21. Rauch, H.E.: Intelligent fault diagnosis and control reconfiguration. IEEE Control Syst. Mag. **14**(3), 6–12 (1994)
22. Salazar, S., Romero, H., Lozano, R., Castillo, P.: Modeling and real-time stabilization of an aircraft having eight rotors. J. Intell. Robot. Syst. **54**(1), 455–470 (2009)
23. Tayebi, A., McGilvray, S.: Attitude stabilization of a vtol quadrotor aircraft. IEEE Trans. Control Syst. Technol. **14**(3), 562–571 (2006)
24. Thau, F.E.: Observing the state of non-linear dynamic systems. Int. J. Control **17**(3), 471–479 (1973)
25. Valavanis, K.P., Gracanin, D., Matijasevic, M., Kolluru, R., Demetriou, G.A.: Control architectures for autonomous underwater vehicles. IEEE Control Syst. Mag. **17**(6), 48–64 (1997)
26. Zhang, X., Polycarpou, M.M., Parisini, T.: Fault diagnosis of a class of nonlinear uncertain systems with lipschitz nonlinearities using adaptive estimation. Automatica **46**(2), 290–299 (2010)